Proceedings of ERAD (2004): 35–40 © Copernicus GmbH 2004

ERAD 2004

Analysis of three-dimensional wind fields from two operational doppler radars

Y. K. Goh and A. R. Holt

Department of Mathematical Sciences, University of Essex, Colchester CO4 3SQ, UK

Abstract. Although methods of using multiple Doppler radars to study wind fields have long been proposed, very few commercial radar operators adopt methods which require the use of specific scanning strategies to allow the extraction of wind information. Here we report a collaborative study on dual-Doppler radars based on two polarimetric radars in the Po valley, Italy. Unusually, the radars are only about 90 km apart, though operated by the same authority. The wind fields synthesis is carried out on a 30 km by 30 km region where the two radars have overlapping scan coverage. An iterative method based on the linear wind model and the equation of mass continuity is used to construct the wind fields. The results have been used to reconstruct the radial winds observed by each separate radar, and these radial winds show good agreement when compared with the original data.

1 Introduction

Modern weather service radars can provide information such as reflectivity, radial Doppler velocity and differential reflectivity. While reflectivity data are commonly used in operational weather forecasting, other data such as Doppler velocity data receive less attention. A workpackage under the European CARPE DIEM project has been set up to improve the use of the Doppler velocity data and attempt to incorporate the information into the routine weather forecasting procedure. A particular interest is to obtain a high resolution three-dimensional wind field using multiple Doppler radars and to channel this into NWP models. This paper reports on progress in dual Doppler wind retrieval (DDWR) using data from two operational northern Italian weather radars.

The theory for multiple Doppler radars wind retrieval has been available for a long time (see Armijo (1969) and Lhermitte (1970)). However, the majority of actual implementations of the multiple Doppler wind retrieval have used research radars which employed specific scanning strategies to allow the retrieval. A more recent attempt (Chong et al. (2000)) involves a French RONSARD research radar and Swiss Meteorological Agency operational radars , and with an emphasis on the retrieval over complex topology.

In this paper, we are performing real-time DDWR analysis on two *operational* weather radars operated by ARPA-SMR, the Italian Emilia-Romagna region weather service agency. This paper is organised as follow: In Sect. 2 we determine the optimal region for performing DDWR analysis. Then, in Sect. 3 we convert the radar data from polar coordinates into rectangular Cartesian coordinates. Section 4 gives the procedure for construction of the wind field and estimation of the accumulated errors. Later, the constructed wind field is verified and two examples are given. Finally, in Sec. 7, we give our conclusions.

2 Terrain Analysis

The terrain around the radars plays an important role for accurate DDWR. The height of the terrain affects the boundary conditions and the lowest elevation angles at which data from the two radars can be used. A flat terrain enables the lower boundary condition to be applied in the continuity equation analysis. Fig. 1 shows the terrain of the Po Valley looking from the east Mediterranean coast of Italy. The north mountain range is the Alps and the south mountain range is the Apennines. In Watson (1996) thesis, he performed retrievals using S. Pietro Capofiume radar and Teolo radar, an Italian Veneto region radar. Due to the high altitude of Teolo radar (∼470 m asl), he had to use a upper boundary condition, where vertical velocity is zero at the top of a mature storm (Browning (1964)).

The preferred area for DDWR is one that lies away from the straight line that connecting the two radars. Ideally this area should at about the same distance from both radars. From Fig. 1 it is clear that the region to the south of the line joining the two radars is not ideal for doing DDWR

Correspondence to: Y. K. Goh
(kygoh@essex.ac.uk)

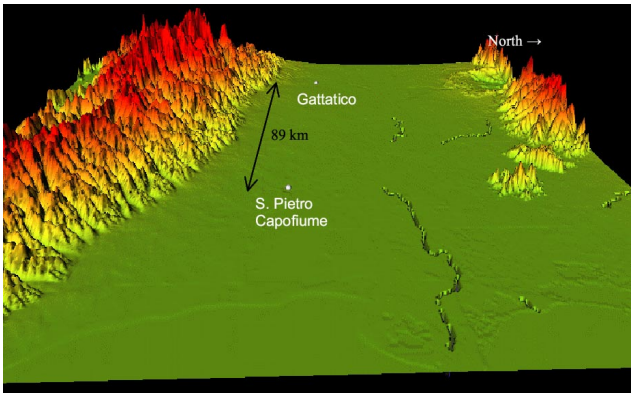

Fig. 1. The Po Valley terrain. The terrain north of the two SMR radars is a flat plain which is ideal for performing dual Doppler wind retrieval. On the other hand, the southern mountain range can contaminate radar measurements with clutter, which make wind retrieval difficult.

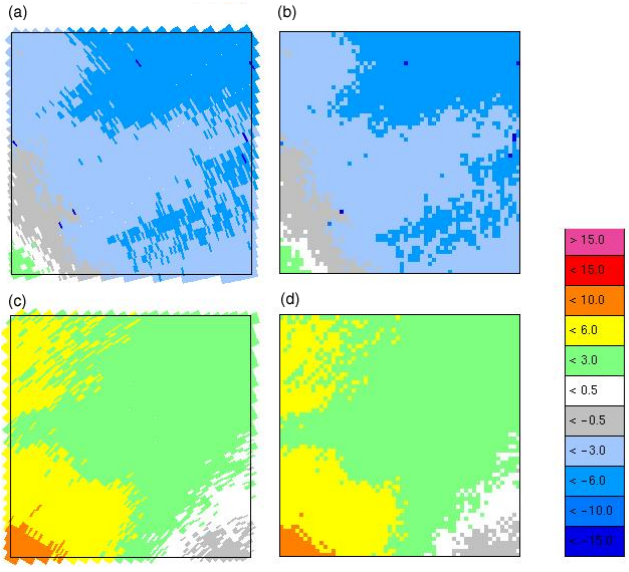

Fig. 2. Data gridding. The left-hand pictures show sections of Doppler velocity PPI scans (2002 Dec 17 1900hrs, elevation angle 1.4°) at the location of wind retrieval area. Picture (a) is from the Gattatico radar and (c) is from the San Pietro Capofiume radar. The right-hand pictures, (b) and (d), show the corresponding gridded data. Most features in the original measured data are preserved in the gridded data. The averaged radial wind speed at Gattatico is −5.31 m/s (standard deviation 2.01 m/s), while in S. Pietro Capofiume it is 2.27 m/s (standard deviation 1.46 m/s).

because of the likelihood of clutter caused by the Apennines for low elevation scans. However, to the north is a flat plain that varies only between 10 m∼30 m. It is an ideal area for DDWR. We therefore chose a 30 × 30 km^2 region with its centre approximately 45 km from the line joining the two radars along its perpendicular bisector.

3 Data Gridding

Before the Doppler radar data can be used for performing DDWR analysis, it has to be converted from Polar coordinates to Cartesian coordinates. We employ a simple algorithm to achieve this data conversion: the chosen area is divided into a rectangular grid, with each cell in the grid having dimension of 0.5 km × 0.5 km. Then, individual pixels (bins) from the radar data which fall inside the grid cell are identified. Each Cartesian cell is assigned the value of the bin falling into that particular cell. If more than one bin falls into the same cell, the value of the cell is the average of those of the bins. Figure 2 is an example of the data conversion, it shows that the conversion retains most of the features of the original data.

4 Wind Field Analysis

Dual Doppler wind retrieval is achieved by solving the standard linear wind field model coupled with the equation of mass continuity

$$\begin{aligned}\hat{\boldsymbol{r}}_{\boldsymbol{i}} \cdot \boldsymbol{v} &= u \sin\alpha_i \cos\phi_i + v \cos\alpha_i \cos\phi_i + w \sin\phi_i \\ &= v_{r_i} - \sin\phi_i W_t \equiv V_i, \quad i = 1, 2 \end{aligned} \tag{1}$$

$$\frac{\partial \rho}{\partial t} + \nabla \cdot (\rho \boldsymbol{v}) = 0, \tag{2}$$

where, $\hat{\boldsymbol{r}}_{\boldsymbol{i}} = \sin\alpha_i \cos\phi_i \boldsymbol{i} + \cos\alpha_i \cos\phi_i \boldsymbol{j} + \sin\phi_i \boldsymbol{k}$ is the unit vector of the direction of ray from the i-th radar; $\boldsymbol{v}(\boldsymbol{r}) = (u, v, w)$ is the wind vector at the location $\boldsymbol{r}$ with u, v and w as the three Cartesian components; α is the azimuth angle clockwise from the north and ϕ is the elevation angle; v_{r_i} is the Doppler velocity measured by i-th radar; V_i is the component of the wind vector towards the radar; and W_t is the terminal velocity of the scatterers. There are several methods to determine W_t, we have chosen the simple relation given by Joss and Waldvogel (1970),

$$W_t = -2.61^{0.0107Z} \tag{3}$$

where W_t is in ms^{-1} and the reflectivity, Z is in dBZ.

The air density $\rho(z)$ is assumed to depend on the vertical height from the ground only. Thus only the gradient in the wind vector and the vertical variation of air density contribute to Eq. (2),

$$\nabla \cdot \boldsymbol{v} + w \frac{\partial}{\partial z}(\ln \rho) = 0. \tag{4}$$

The vertical density variation factor $\Gamma \equiv \partial(\ln\rho)/\partial z$ in Eq. (4) is roughly -0.0001 m^{-1} for a typical stratified atmosphere.

Eq. (1) and Eq. (4) are then solved by using an approach similar to that described in Dowell and Shapiro (2003). Two horizontal components of the wind vector are expressed in terms of the vertical component of the wind vector by inverting the linear wind equations (Eq. 1) of the individual radars:

$$u = A + Bw \tag{5}$$

$$v = C + Dw, \tag{6}$$

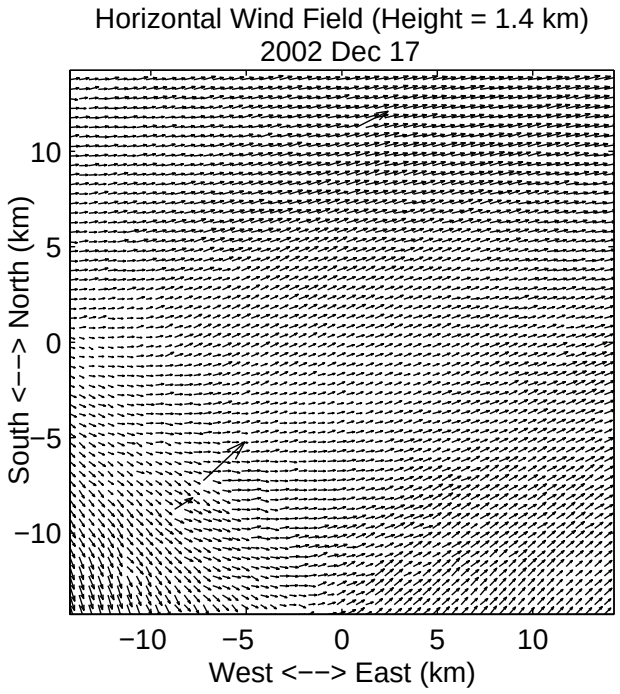

Fig. 3. Retrieved wind field. Only horizontal components are shown here. It is clear that wind is generally travelling in the north-east direction. Also, the wind field is fairly uniform and this allows us to perform a VAD analysis, which is shown in Fig. 4.

where B and D are constants depending only on the azimuths and the elevation angles, and A and C are constants that depend not only on the azimuths and the elevation angles but also on the radial wind velocities toward the radars. The vertical component of the wind vector is calculated by discretising Eq. (4) to give

$$\left(1+\frac{\Gamma\Delta z}{2}\right)w_k = \left(1-\frac{\Gamma\Delta z}{2}\right)w_{k-1} - \left(\frac{\partial u}{\partial x}+\frac{\partial v}{\partial y}\right)\Delta z. \quad (7)$$

Here the horizontal components of the velocity gradient are averaged over two different heights, e.g. $\frac{\partial u}{\partial x} = \frac{1}{2}\left(\frac{u_{i+1,j,k}-u_{i-1,j,k}}{2\Delta x} + \frac{u_{i+1,j,k-1}-u_{i-1,j,k-1}}{2\Delta x}\right)$. In our calculation, we have used the horizontal spacing $\Delta x = \Delta y = 0.5$ km and the vertical spacing $\Delta z = 0.9$ km.

Due to the lack of information about the upper boundary layer, we chose to iterate Eq. (7) from the bottom layer to the top. The boundary conditions used assume the vertical component of the wind on the surface to be zero and the horizontal components to have zero local gradient, i.e. $\frac{\partial u}{\partial x}\big|_{k=0} = \frac{\partial v}{\partial y}\big|_{k=0} = 0$. The imposed zero horizontal wind gradient condition on the ground is optional and can be relaxed if one uses the forward finite difference method, instead of the centre finite difference method, to calculate w_k for the first layer. We chose to have this condition here simply for the ease of programming.

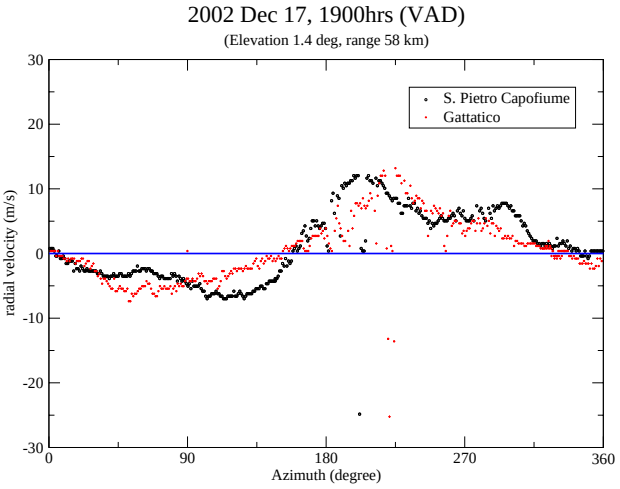

Fig. 4. VAD diagram from two SMR radars. Maximum radial velocity at the azimuth of approximately 225° indicate wind is travelling in the north-east direction, is in agreement with Fig. 3.

The error at the n-th iteration in the solution of $w^{(n)}_{i,j,k}$ is defined by

$$\epsilon^{(n)} = w^{(n)} - w^{(n-1)}. \quad (8)$$

The convergence factor λ is defined as the ratio of the error at n-th and $(n-1)$-th iterations:

$$\lambda \equiv \frac{F^{(n)}}{F^{(n-1)}} = -\left(1+\frac{\Gamma\Delta z}{2}\right)^{-1} \left\{\frac{\Delta z}{4\,\Delta x}\left(B_{i+1,j,k}e^{ir\Delta x} - B_{i-1,j,k}e^{-ir\Delta x}\right) + \frac{\Delta z}{4\,\Delta y}\left(D_{i,j+1,k}e^{is\Delta y} - D_{i,j-1,k}e^{-is\Delta y}\right)\right\}. \quad (9)$$

Here $F^{(n)}$ is the amplitude of the Fourier component of error, and r and s are the wavenumbers. In our calculations, we assumed that B and D do not vary horizontally. The calculated value of the convergence factor is typically 0.03 for a scan with elevation angle of 0.5°.

5 Uniform Wind Field (Case study: 2002 Dec 17)

The retrieved wind field is a 3-dimensional vector field, but it is often easier to interpret by looking at the 2-dimensional projection of the wind field. Figure 3 shows an example of horizontal components of the retrieved wind field. It is clear that the wind is generally travelling in the north-east direction. Three long arrows in Fig. 3 are caused by the unusual strong Doppler wind measurements (cf. Fig. 2), which very likely are noise.

Figure 4 shows the VAD (Velocity Azimuth Display) plots at the range of 58 km from both radars. The VAD range corresponds to the distance of the centre of the retrieval area from the radars. The peaks of the VAD plots are approximately 13 m/s at the azimuth of 225°. The SMR radars adopt

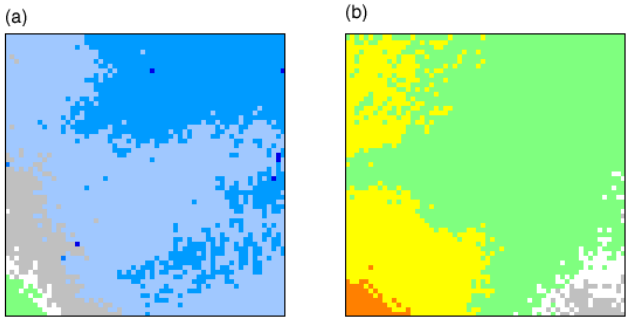

Fig. 5. Re-construction of radial winds. (a) is the reconstruction of retrieved radial wind (average speed = −5.20 m/s, standard deviation 2.03 m/s) as seen from Gattatico radar, while (b) is the corresponding reconstructed radial wind (average speed = 2.38 m/s, standard deviation 1.46 m/s) as seen from S. Pietro Capofiume.

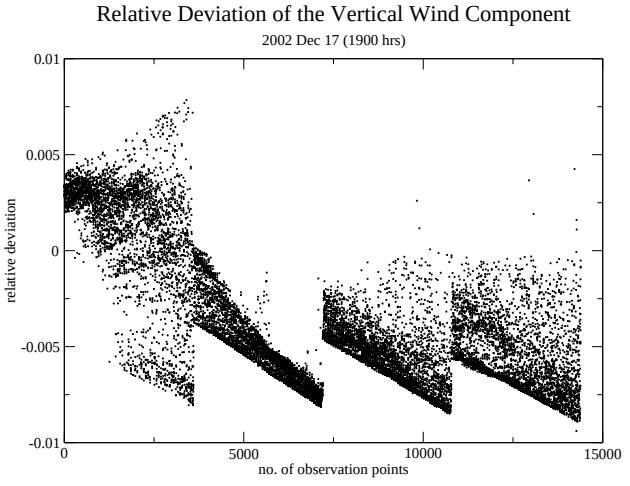

Fig. 6. This shows the relative deviation of the calculated wind component along the line joining the two radars (along-track component). The relative deviation of the along track component is typically not more than ±1%.

the convention that positive radial velocity implies movement towards the radars. This suggests that the wind is travelling from the south-west direction, which is in agreement with the retrieved wind field.

To verify that the retrieved wind field is indeed correct, we first use the retrieved wind field to re-construct the radial wind as seen from the SMR radars. Figure 5 shows the reconstruction of the radial winds toward the Gattatico radar (Fig. 5a) and S. Pietro Capofiume radar (Fig. 5b) using the data illustrated in Fig 3. Comparion of Fig. 5a with the top panel of Fig. 2 and of Fig. 5b with the bottom panel of Fig. 2 show a very close match between the re-constructed radial wind with the original measurements.

Another verification comes from the calculation of the along-track component of the retrieved wind field. Let $\boldsymbol{r}_1$ and $\boldsymbol{r}_2$ be the position vectors of the resolution volume from the first and second radar respectively, and let $\boldsymbol{r}_{12} = \boldsymbol{r}_1 - \boldsymbol{r}_2$.

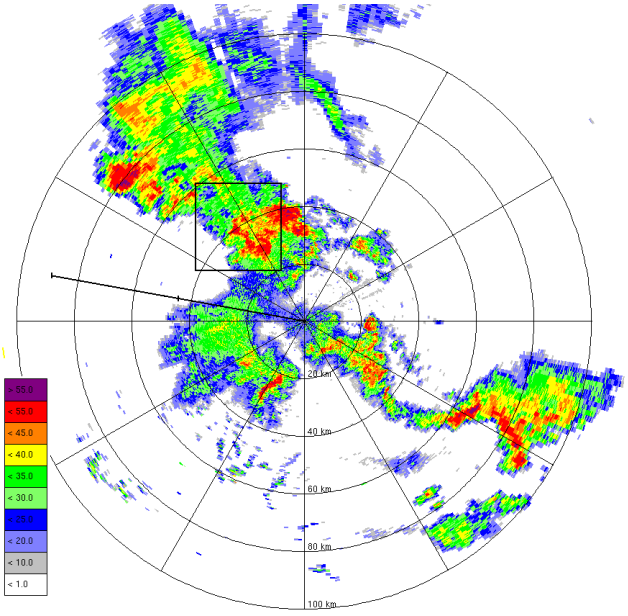

Fig. 7. Reflectivity PPI picture of S. Pietro Capofiume radar at the elevation angle of 1.4°. Two ends of the straight line are the locations of the two radars used for DDWR. The retrieval area is shown by the square box, where a circulation pattern is visible on the lower right of the box (cf. Fig. 8).

Then,

$$\boldsymbol{v} \cdot (\boldsymbol{r}_{12} + \boldsymbol{r}_2 - \boldsymbol{r}_1) = 0. \tag{10}$$

For every cell in the retrieval area, we have the radial velocity measurements V_i and we know the distances $|\boldsymbol{r}_i|$ from both radars. We also know the distance between the radars. Together with the retrieved wind vector, we can calculate

$$\Delta = \boldsymbol{v}^{(cal)} \cdot \boldsymbol{r}_{12} + V_2^{(obs)} \times |\boldsymbol{r}_1| - V_1^{(obs)} \times |\boldsymbol{r}_2|. \tag{11}$$

The superscripts emphasis that $\boldsymbol{v}^{(cal)}$ is the retrieved (calculated) wind vector and $V_i^{(obs)}$ is a radar measurement. If the DDWR produced a perfect wind field, then Δ would be zero.

Figure 6 shows a graph of $\Delta/|v||\boldsymbol{r}_{12}|$ against individual observation point. It shows that the relative deviation of calculated along-track component from the observation value is within ± 1%. The consistent increasing of the magnitude of the relative deviation is caused by the accumulation of errors in calculating the vertical wind component. The accumulation drops when the calculation of the vertical wind component moves to the next value of height.

6 Convective Storm (Case study: 2003 Jul 31)

In the case of non-uniform wind fields, the DDWR method gives results which are more reliable than those obtained by the widely used VAD analysis. Figure 7 shows a reflectivity PPI on 31 July 2003 captured by S. Pietro Capofiume radar. We have set the retrieval area to be at the location specified by the square on the PPI picture. The retrieval area now covers

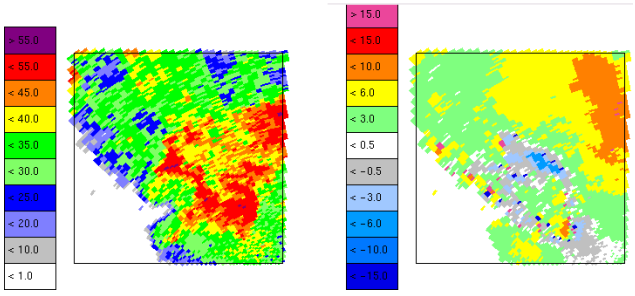

Fig. 8. The close-up view of the box in Fig. 7. To the left is the reflectivity PPI and to the right Doppler velocity PPI. The opposite signs of the Doppler velocity measurements in the right picture indicates possible rotation.

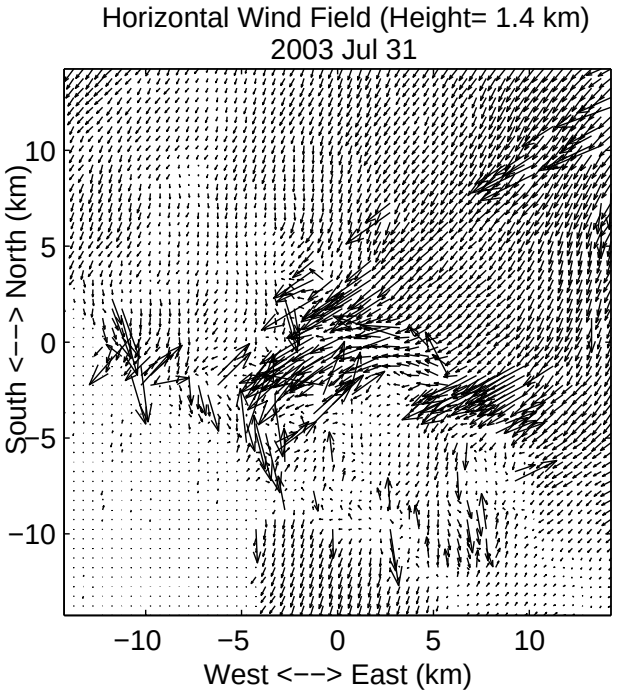

Fig. 9. Retrieved wind field on 31 July 2003. Note that some arrows actually oppose the general wind field.

part of an intense convective storm where the wind field is highly non-uniform.

Figure 9 shows the retrieved wind field from the Gattatico radar and S. Pietro Capofiume radar at the retrieval area specified in Fig. 7. In this case, the retrieved wind field is far from uniform. The opposite direction of wind arrows on the lower right hand corner area suggesting possible turbulence vortices caused by a convective storm in this area. In this situation, the VAD analysis, which is based on a uniform wind field assumption, breaks down and cannot give the useful information about the wind field (cf. Fig. 10).

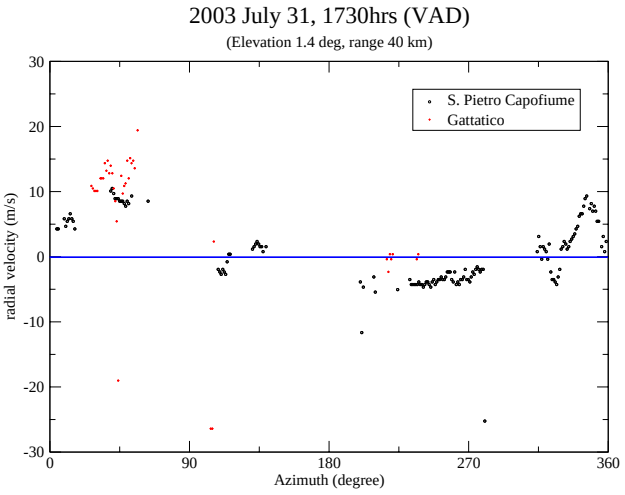

Fig. 10. VAD diagram from two SMR radars at the VAD range of 40 km. The missing radial points correspond to the white area in Fig. 7.

7 Conclusions

In this paper, we have successfully retrieved three-dimensional wind fields, albeit only shown as two-dimensional, from two operational Doppler radars at Po Valley. We have written a computer program capable of displaying the 3-dimensional wind field in real-time. This might actually allow DDWR to go into operational use for radar operators to provide detailed wind fields, and not just the radial wind components.

We selected the radar data from 2002 Dec 17 as an example for the study because in this day the wind field is relatively uniform. This makes it possible to compare the direction of the retrieved wind field with the VAD analysis. The agreement confirms the accuracy of the DDWR procedure.

VAD analysis is used widely to give wind information from Doppler radar, but the analysis breaks down if the wind field is highly non-uniform or localised like some convective cells. Figure 9 shows that DDWR can be a valuable tool for radar operators providing useful information when a VAD analysis is not viable.

Acknowledgements. This research is part of the CARPE DIEM project (contract no EVG1-CT-2001-0045), which is supported by the European Commission under the Fifth Framework Programme.

References

Armijo, L.: A Theory for Determination of Wind and Precipitation Velocities with Doppler Radars, J. Atmos. Sci., 26, 570–570, 1969.

Browning, K. A.: Airflow and precipitation trajectories within severe local storm which travel to the right of the winds, J. Atmos. Sci., 21, 634–639, 1964.

Chong, M., Georgies, J. F., Bousquet, O., Brodzik, S. R., Burghart, C., Cosma, S., Germann, U., Gouget, V., Jr., R. A. H., James,

C. N., Prieur, S., Rotunno, R., Roux, F., Vivekanandan, J., and Zeng, Z. X.: Real-time wind synthesis from Doppler radar observations during the Mesoscale Alpine Programme, Bulletin Amer. Meteor. Soc., 81, 2953–2962, 2000.

Dowell, D. C. and Shapiro, A.: Stability of an Iterative Dual-Doppler Wind Synthesis in Cartesian Coordinates, J. Atmos. Oceanic Technol., 20, 1552–1559, 2003.

Joss, J. and Waldvogel, A.: Raindrop size distribution and Doppler velocities, in Preprint, 14th Conf. on Radar Meteorology, pp. 153–156, Amer. Meteor. Soc., 1970.

Lhermitte, R. M.: Dual-Doppler radar observations of convective storm circulation, in Preprint, 14th Conf. on Radar Meteorology, pp. 153–156, Amer. Meteor. Soc., 1970.

Watson, R. J.: Data Comparisons for Spatially Separated Meteorological Radars, Phd thesis, Department of Electronic Systems Engineering, University of Essex, Department of Electronic Systems Engineering, University of Essex, 1996.